Spin-Order-Induced Ferroelectricity and Magnetoelectric Effect in $LiCuFe_2(VO_4)_3$

Anatoly V. Koshelev,[1] Konstantin V. Zakharov,[1] Alexander P. Pyatakov,[1] Larisa V. Shvanskaya,[1,2] Alexander A. Shakin,[2] Olga S. Volkova,[1,2,3] Dmitry A. Chareev,[3,4] Sirko Kamusella,[5] Hans-Henning Klauss,[5] Kaimujjaman Molla,[6] Badiur Rahaman,[6] Tanusri Saha-Dasgupta,[7,8] and Alexander N. Vasiliev[1,2,9,*]

[1]*Lomonosov Moscow State University, 119991 Moscow, Russia*
[2]*National University of Science and Technology "MISiS," 119049 Moscow, Russia*
[3]*Ural Federal University, 620002 Ekaterinburg, Russia*
[4]*Institute of Experimental Mineralogy, RAS, 142432 Chernogolovka, Russia*
[5]*Dresden Technical University, 01062 Dresden, Germany*
[6]*Aliah University, 700156 Kolkata, India*
[7]*S.N. Bose National Centre for Basic Sciences, 700098 Kolkata, India*
[8]*Indian Association for the Cultivation of Science, Jadavpur, 700032 Kolkata, India*
[9]*National Research South Ural State University, 454080 Chelyabinsk, Russia*

(Received 19 November 2017; revised manuscript received 21 June 2018; published 6 September 2018)

The mixed spin chain compound, $LiCuFe_2(VO_4)_3$, reaches a magnetically ordered state in two steps at $T_{N2} = 9.8$ K and $T_{N1} = 8.2$ K detected in magnetic-susceptibility χ and specific-heat C_p measurements. Dielectric permittivity ε evidences these transitions by a sharp peak at T_{N2} and a steplike anomaly at T_{N1}, both easily suppressed by an external magnetic field. These features in permittivity are preceded by a frequency-dependent relaxation-type anomaly at T^* insensitive to the magnetic field. Mössbauer spectroscopy reveals a wide distribution of a hyperfine field between T_{N2} and T_{N1} while the first-principles calculations provide values of magnetic-exchange-interaction parameters. For Cu, the orbital moment aligned in the same direction as the spin moment is substantial. This large orbital moment is important in driving the polarization through an inverse Dzyaloshinksii-Moriya interaction in a situation where the spatial symmetry gets broken in the magnetic structure. The data obtained suggest the spin-order-induced ferroelectricity is inherent for improper multiferroics.

DOI: 10.1103/PhysRevApplied.10.034008

I. INTRODUCTION

The coexistence of ferroelectricity and magnetism has been considered a mutually exclusive phenomenon for a long time [1], but now represents a flourishing field of magnetoelectric multiferroicity [2–4]. Quite a number of physical mechanisms may justify the coexistence (and coupling) of these order parameters in a single homogeneous material [5–8]. Phenomenologically, magnetoelectric multiferroics can be divided in two classes: type-I multiferroics with a ferroelectric Curie point higher than the magnetic ordering temperature, and type-II (or improper) multiferroics with a magnetically induced electric polarization appearing below magnetic Curie or Neel temperature [9]. In particular, the magnetoelectric coupling is an intrinsic feature of the improper multiferroics where the ferroelectric polarization arises from spiral magnetic ordering [10–13]. The spirals are the result of competition of the nearest-neighbor and higher-order super-exchange-interactions. Thus, choosing a compound with the appropriate bond angles in three-ion clusters (transition-metal ion–ligand–transition-metal ion) allows one to fine tune the balance between the exchange interactions by varying the temperature. The case of CuO, which reaches collinear long-range magnetic order through a succession of phase transitions at $T_{N1} = 213$ K and $T_{N2} = 230$ K with an incommensurate spiral structure between these temperatures, is instructive [14]. The phase transition at T_{N2} is marked by a sharp peak in dielectric permittivity reflecting the formation of a ferroelectric phase.

Here, we report on spin-order-induced ferroelectricity and a magnetoelectric effect in $LiCuFe_2(VO_4)_3$, which is isostructural to howardevansite mineral $NaCuFe_2(VO_4)_3$ [15]. In many respects, the howardevansites differ from any magnetoelectric material studied so far. Their magnetic subsystem is represented by two types of 3*d* transition metals, Cu and Fe, with a third 3*d* transition metal, V, being magnetically silent. The alkali metals are subject to

*vasil@mig.phys.msu.ru

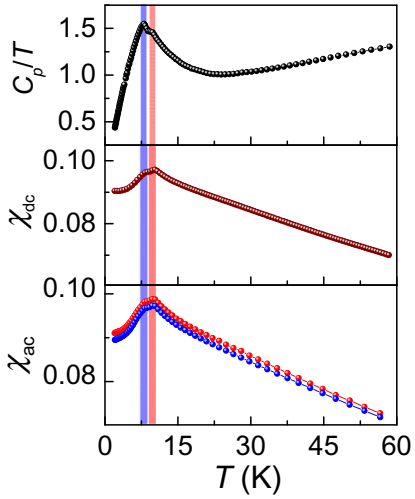

FIG. 1. The temperature dependences of specific heat C_p/T, dc susceptibility χ_{dc}, and ac susceptibility χ_{ac} in $LiCuFe_2(VO_4)_3$.

hopping within the tunnels of crystal structure. Belonging to the space group $P\bar{1}$, $LiCuFe_2(VO_4)_3$ may serve as an example of a type-II multiferroic medium with the lowest possible symmetry of paraelectric and magnetoelectric phases: the only symmetry element is the inversion center that is broken at the Neel temperature. The synthesis and physical properties of $LiCuFe_2(VO_4)_3$ were reported in Ref. [16]. It was concluded that this compound is a kind of quasi-one-dimensional antiferromagnet. No evidence for spin-order-induced ferroelectricity and a magnetoelectric effect were presented.

II. EXPERIMENT

$LiCuFe_2(VO_4)_3$ has a triclinic primitive cell with two formula units per unit cell, consisting of two inequivalent iron atoms, Fe1 and Fe2, which are situated at the center of a distorted oxygen octahedra, and one Cu atom, which is at the center of a distorted oxygen trigonal bipyramid. In the structure, two $Fe1O_6$ octahedra share a common edge and form $Fe1O_6$ dimers. The dimers of $Fe2O_6$ octahedra form in a similar way. These dimers are connected by edge sharing via CuO_5 bipyramids constituting an Fe1-Fe1-Cu-Fe2-Fe2 mixed spin chain. The chains are connected by VO_4 tetrahedra forming a three-dimensional network. The Li^+ ions occupy the channels of this structure. One position of the two alkali ions is half-filled, which opens the way to cooperative hopping within the channels.

The powder sample of $LiCuFe_2(VO_4)_3$ has been synthesized by the solid-state reaction of Li_2CO_3, Fe_2O_3, CuO, and V_2O_5, as described in Ref. [17]. The reagents are taken in stoichiometric ratio, homogenized in an agate mortar, placed into the alumina crucible, and burned in two steps in air at 600 °C and 640 °C for 72 h with intermediate grinding. The crystalline quality and phase purity of the sample are confirmed by the powder XRD method.

The thermodynamic properties of $LiCuFe_2(VO_4)_3$, i.e., specific heat C_p, ac and dc susceptibility χ, are investigated in the range 2–300 K using the relevant options of the "Quantum Design" Physical Properties Measurements System (PPMS) – 9T. Dielectric permittivity ε is measured at several frequencies in the kHz range by means of a capacitance bridge (Andeen-Hagerling 2700A). Mössbauer spectroscopy is done with a standard Wissel setup using a ^{57}Co source with a line width of 0.107 mm/s. The drive is run in sinusoidal mode minimizing the velocity error. The measurements are carried out in an Oxford continuous-flow cryostat in the under pressure mode. The spectra are analyzed using the Moessfit algorithm by means of transmission integral fits [18].

III. MAGNETIC SUSCEPTIBILITY AND SPECIFIC HEAT

The temperature dependences of specific heat C_p/T, dc susceptibility χ_{dc}, and ac susceptibility χ_{ac} in $LiCuFe_2(VO_4)_3$ are shown in Fig. 1. The compound experiences long-range antiferromagnetic order at low temperatures accompanied by distinct anomalies in both C_p and χ. In the range 150–300 K, the parameters of the paramagnetic subsystem are estimated according to the Curie–Weiss law,

$$\chi = \chi_0 + \frac{C}{T - \Theta}, \tag{1}$$

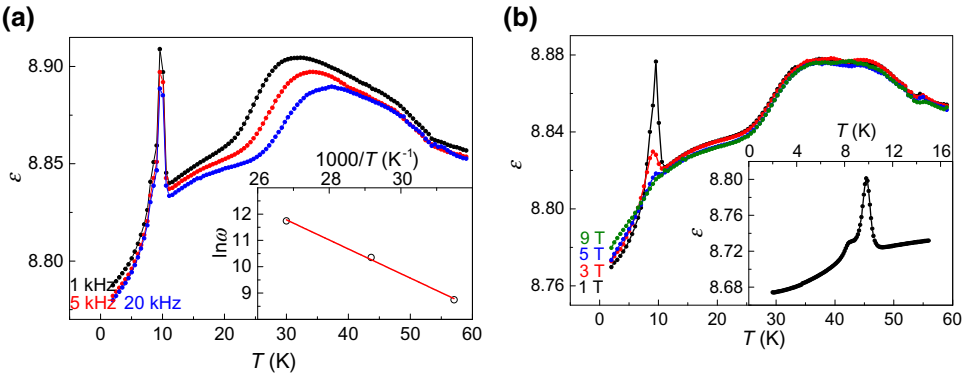

FIG. 2. Dielectric permittivity ε in $LiCuFe_2(VO_4)_3$. The ε probed at various frequencies f. The inset represents the Arrhenius plot (left panel). The ε probed at various magnetic fields at $f = 20$ kHz. The inset enlarges the low-temperature section of the $\varepsilon(T)$ curve (right panel).

where $\chi_0 = -7.0 \times 10^{-4}$ emu/mol results from the balance of diamagnetic Pascal constants [19] and paramagnetic Cu^{2+} van Vleck contribution [20]. The value of the Curie constant $C = 9.2$ emu/mol K is consistent with the notion of the Cu^{2+} ($S = 1/2$) and Fe^{3+} ($S = 5/2$) moments. The large negative value of the Weiss temperature $\Theta = -80$ K indicates the predominance of antiferromagnetic interactions in the system.

Compared to the Weiss temperature, the ordering temperature in $LiCuFe_2(VO_4)_3$ is rather low pointing to the reduced dimensionality of the magnetic subsystem and/or competition of various exchange interactions. At low temperatures, the C_p/T vs T curve shows two separated peaks in close vicinity. This two-peak structure of magnetic singularity is further confirmed in measurements of dc and ac susceptibility. The upper- and lower-peak temperatures are $T_{N2} = 9.8$ K and $T_{N1} = 8.2$ K, respectively. No difference between $\chi_{dc}(T)$ curves in zero-field-cooled and field-cooled protocols is detected suggesting an absence of appreciable spin-glass or disorder effects. The $\chi_{ac}(T)$ curves taken at various frequencies do not evidence any qualitative difference.

IV. DIELECTRIC PERMITTIVITY AND MAGNETOELECTRIC EFFECT

On lowering the temperature, the dielectric permittivity ε in $LiCuFe_2(VO_4)_3$ exhibits a broad frequency-dependent relaxor-type anomaly at $T^* \sim 30$ K, a sharp peak at T_{N2}, and a steplike feature at T_{N1} as shown in Fig. 2. The broad anomaly at T^* can be ascribed to the formation of polar nanoregions as is typically observed in relaxor ferroelectrics [21]. However, the relaxor-type phenomenology based on quenched internal random electric fields can be excluded because of a lack of static charge disorder. Alternatively, this feature can be attributed to cooperative hopping of Li^+ ions within the channels of crystal structure [22]. Its characteristic temperature shifts upward with frequency following the Arrhenius plot with activation energy $\Delta_{act} \sim 0.06$ eV, as shown in the inset in the left panel of Fig. 2. The activation energy for cooperative hopping is an order of magnitude smaller than that established for intragrain and intergrain hoppings in $LiCuFe_2(VO_4)_3$ ceramics at elevated temperatures [23]. The broad maximum in dielectric permittivity is insensitive to the external magnetic field, but the field rapidly suppresses the singularities at T_{N2} and T_{N1}. The pronounced magnetoelectric effect at the formation of the magnetically ordered phase is a signature of improper multiferroicity. The overall appearance of sharp singularities in the $\varepsilon(T)$ curve in $LiCuFe_2(VO_4)_3$, as shown in the inset in the right panel of Fig. 2, is reminiscent of that in CuO, where it is associated with the formation of incommensurate magnetic structure at T_{N2} and subsequent incommensurate-commensurate phase transition at T_{N1} [14].

V. MÖSSBAUER SPECTROSCOPY

The Mössbauer spectra of $LiCuFe_2(VO_4)_3$, taken at various temperatures both in paramagnetic- and magnetically-ordered states, are shown in the upper panel of Fig. 3. A two-site model is applied to reproduce the data. Both sites are based on the static Hamiltonian,

$$H_s = \frac{eQ_{zz}V_{zz}}{4I(2I-1)}\left[(3I_z^2 - I^2) + \frac{\eta}{2}(I_+^2 + I_-^2)\right] - g_I\mu_N B\left(\frac{I_+e^{-i\Phi} + I_-e^{+i\Phi}}{2}\sin\Theta + I_z\cos\Theta\right) \quad (2)$$

sharing the same isomer shift. For the electric field gradient (EFG) axial symmetry is assumed, $\eta = 0$. The angle between the EFG z axis and B_{hyp} is 90° in this model. The principal component of EFG is assumed to be temperature independent and the same for both sites $V_{zz} = -39$ V/Å$^2 = 0.65$ mm/s.

The spectra require a real distribution of a static magnetic hyperfine field B_{hyp} because at base temperature (2 K) they already show a strongly asymmetric line shape. The analysis is done in a purely static picture using the following theory:

$$\begin{aligned} m &\in [-1,1]; \quad \sigma \in [0, B_0/(1/2 + m/6)]; \\ B_{min} &= B_0 - (1/2 + m/6)\sigma; \\ B_{max} &= B_0 + (1/2 - m/6)\sigma; \\ x &= \frac{B_{hyp} - B_{min}}{B_{max} - B_{min}} \Rightarrow x \in [0,1]; \\ y_0 &= (1-m); \quad \rho(x) = 2mx + y_0; \\ \langle B_{hyp}\rangle &= B_{hyp}(\langle x\rangle) \\ &= B_{hyp}\left[\int_0^1 x\rho(x)dx\right] \\ &= B_{hyp}(x = 1/2 + m/6) = B_0. \end{aligned} \quad (3)$$

This distribution is linear in B_{hyp} and can change its weight from lower fields ($m = -1$) to higher fields ($m = +1$). Thus, the distribution is parametrized by the mean value B_0, the distribution width σ, and the skewness m. This model can roughly satisfy all Mössbauer spectra. To quantitatively describe the Mössbauer spectra in both compounds, we introduce an impurity sextet, which is still present at room temperature. Its fraction weight is about 5% in $LiCuFe_2(VO_4)_3$.

The data indicate substantial changes in the field distribution by the change of the skewness m from -1 to $+1$ at about 8.2 K. The low-temperature isomer shift with respect to room-temperature iron is $\delta(T \to 0) \approx 0.5$ mm/s. The model roughly fits the data and provides a temperature dependence of the parameters B_0 and σ, as shown in the middle panel of Fig. 3. The nonmonotonic behavior of

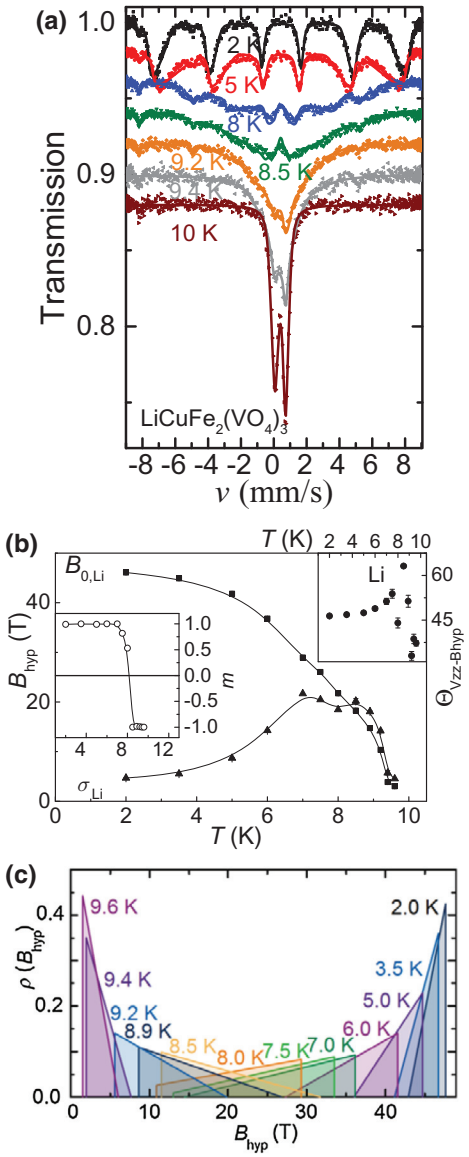

FIG. 3. The temperature evolution of the Mössbauer spectra in $LiCuFe_2(VO_4)_3$. The solid lines are the fits with static field distribution, as given by Eq. (3) (upper panel). The magnetic hyperfine field distribution modeled with Eq. (3) (middle panel). The distributions of hyperfine field at ^{57}Fe nuclei at various temperatures within the T_{N1}–T_{N2} range (lower panel).

the width parameter σ is evident in the range between T_{N2} and T_{N1}. A plot sketching the modeled field distribution in $LiCuFe_2(VO_4)_3$ at various temperatures in the range between T_{N2} and T_{N1} is shown in the lower panel of Fig. 3. This kind of hyperfine field distribution at ^{57}Fe is consistent with the incommensurate-commensurate scenario suggested by $\varepsilon(T)$ data.

VI. FIRST-PRINCIPLES CALCULATIONS

In order to gain microscopic understanding of $LiCuFe_2(VO_4)_3$, the first-principles density-functional-theory (DFT) calculations [24] within the generalized gradient approximation (GGA) for the exchange-correlation functional are carried out [25]. Calculations use a plane-wave basis as implemented within the Vienna Ab initio Simulation Package (VASP) [26] as well as muffin-tin orbital (MTO)-based Nth-order MTO (NMTO) [27], and linear MTO (LMTO) [28], which are implemented in Stuttgart code. The effect of the coulomb correlation beyond GGA at Fe and Cu sites is handled within the supplemented +U correction of GGA + U [29]. The consistency of the obtained results between the MTO basis-set calculations and plane-wave basis-set calculations is checked in terms of ground-state electronic structures.

Nonspin-polarized self-consistent calculations are carried out for the $LiCuFe_2(VO_4)_3$ compound. The states close to the Fermi level are predominantly of the Fe d and Cu d characters with an admixture of the O p character due to finite Fe-O and Cu-O covalencies. Thus, the Fe d and Cu d states at the Fermi level are primarily responsible for the electronic and magnetic properties. The corresponding spin-polarized density of states, obtained in a self-consistent spin-polarized DFT calculation and projected onto Fe d, Cu d, O p, V d, and Li s states, indicates that the Fe d states are completely filled in the majority spin channel and completely empty in the minority channel suggesting the nominal Fe^{+3} or d^5 valence state of Fe. Meanwhile the Cu d states are completely filled in the majority and minority spin-channels except for the minority channel of Cu d_{x2-y2} suggesting the nominal Cu^{+2} or d^9 valence of Cu. The O p state is found to be mostly occupied suggesting the nominal O^{-2} valence states. The O p state shows finite, nonzero hybridization with Fe d and Cu d states close to the Fermi energy, which contributes to the super-exchange-paths of the magnetic interaction. The oxidation states of Li and V ions are +1 and +5, respectively. Additional calculations including spin-orbit coupling are carried out considering collinear as well as noncollinear arrangements of magnetic moments. Starting with the

TABLE I. The calculated magnetic moment (in μ_B) at different sites of $LiCuFe_2(VO_4)_3$ as obtained in GGA + U ($U_{cu} = 4$ eV, $U_{Fe} = 8$ eV, $J_H = 0.8$ eV) and in GGA + U + SOC (shown in parenthesis). For the GGA + U + SOC calculation, the spin and orbital moments in the x, y, and z directions are shown. For the Li site, the magnetic moment is found to be vanishing in both calculations.

Cu	Fe	V	O	Li
0.66 (0.01, 0.03, 0.62; 0.02, 0.05, 0.08)	4.59 (0.00, 0.00, 4.58; 0.00, 0.00, 0.01)	0.12 (0.02, 0.01, 0.10; 0.00, 0.00, 0.02)	0.12 (0.02, 0.02, 0.11; 0.00, 0.00, 0.02)	0.00

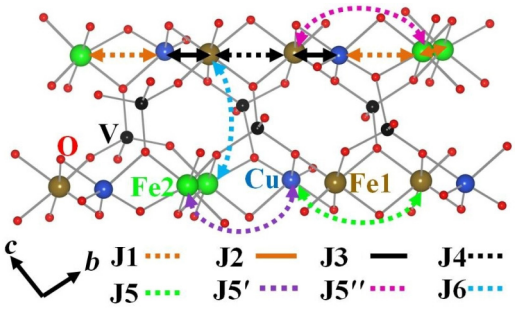

FIG. 4. The interaction pathways for dominant magnetic exchange interactions J1–J6 in $LiCuFe_2(VO_4)_3$.

collinear alignment of the spin and orbital moment having moments pointed along the z direction, relaxation within the noncollinear GGA + U + SOC (spin-orbit coupling) calculations is found to produce nonzero components in the x and y directions (cf. Table I) asserting the presence of finite spin-orbit coupling, especially at the Cu site. The magnitude of the orbital moment at the Cu site is found to be a nonnegligible value of about 0.1 m_B. This large orbital moment will be important in driving the polarization through an inverse Dzyaloshinksii-Moriya interaction in the situation where the spatial symmetry gets broken in the magnetic structure. Table I also lists the moment obtained from GGA + U in the absence of any spin-orbit coupling. The difference of the two also emphasizes the relative importance of the spin-orbit coupling.

VII. MAGNETIC INTERACTIONS

In order to estimate the various Cu-Cu, Fe-Fe, and Cu-Fe magnetic exchange interactions as well as the crystal field splitting of different d orbitals of Fe and Cu, a NMTO-based downfolding technique is applied to construct Fe d and Cu d_{x2-y2} Wannier functions by downfolding all the degrees of freedom associated with O, V, and Li and keeping active only the Fe d and Cu d_{x2-y2} degrees of freedom. This procedure provides renormalization of the Fe d and Cu d_{x2-y2} orbitals due to hybridization from O p, V d, Li s, and the other Cu d orbitals. The effective Fe-Fe, Fe-Cu d_{x2-y2}, and Cu d_{x2-y2}-Cu d_{x2-y2} hopping interactions are obtained from the real-space representation of the Hamiltonian in the effective Fe d and Cu d_{x2-y2} Wannier function basis. The strengths of hopping interactions provide information on dominant Fe-Fe, Fe-Cu, and Cu-Cu magnetic interactions. In principle, the magnetic interactions can be calculated from the knowledge of the hopping interactions and crystal field splitting, together with the choice of the Hubbard U parameter in the super-exchange-formula. This procedure, however, only accounts for the antiferromagnetic contributions. Thus, to obtain a more reliable estimate of magnetic exchanges, we perform the total energy calculation of different spin configurations in the GGA + U scheme and extract the dominant magnetic exchanges by mapping the DFT energies to that of the Heisenberg model. The GGA + U calculations are performed for the choice of U = 8 eV. The spin chain formed by Fe1, Fe2, and Cu spins and the paths for dominant magnetic interactions for the $LiCuFe_2(VO_4)_3$ compound are shown in Fig. 4. The calculated values of the magnetic exchanges are listed in Table II.

Focusing on the calculated magnetic interactions, we notice that interchain interactions are an order of magnitude smaller compared to the dominant nearest-neighbor intrachain interactions, suggesting a weakly coupled spin chain model of the compounds. Note, our calculation does not take into account the possible mobility of Li^+ ions within the channel, which can modulate the magnetic interactions. We find the dominant magnetic interactions to be of an antiferromagnetic nature, although weaker ferromagnetic interactions are also present. This may give rise to a complex magnetic ground state.

VIII. CONCLUSIONS

At the renaissance of multiferroicity in the beginning of this century, it was conjectured that many new magnetoelectric and multiferroic oxides exhibiting magnetically induced ferroelectricity would be found [30]. In part, this is true, but it was found at the same time that these phenomena are quite rare. It seems that $LiCuFe_2(VO_4)_3$ belongs to this family. The magnetic subsystem in $LiCuFe_2(VO_4)_3$ is quite peculiar in that it is constituted by weakly coupled chains of mixed spins. Within chains, these spins are coupled by multiple antiferromagnetic and

TABLE II. Magnetic-exchange-interaction parameters in $LiCuFe_2(VO_4)_3$.

Interaction	Path	Bond angles	Bond distance (Å)	Value (meV)
Nearest-neighbor intrachain	J1 (Cu-O-Fe2)	99.9° and 99.2°	3.074	−0.11
	J2 (Fe2-O-Fe2)	104.2° and 104.9°	3.112	1.02
	J3 (Cu-O-Fe1)	98.4° and 103.7°	3.121	1.08
	J4 (Fe1-O-Fe1)	103.5° and 104.4°	3.156	1.38
Next-nearest-neighbor intrachain	J5 (Cu-O-Fe1-O-F1)	–	5.122	−0.09
	J5′ (Cu-O-Fe2-O-F2)	–	5.150	−0.01
	J5″ (Fe1-O-Cu-O-Fe2)	–	5.114	0.05
Interchain	J6 (Fe1-O-V-O-Fe2)	–	4.753	0.11

ferromagnetic exchange interactions, which open the way to the formation of noncollinear structures, either commensurate or incommensurate. The latter ones break the spatial inversion symmetry of the compound. Sharp singularities in dielectric permittivity ε at phase transitions at T_{N2} and T_{N1} and their sensitivity to the magnetic field prove the spin-order-induced ferroelectricity in this compound. The magnetoelectric effect and hyperfine field distribution are consistent with the formation of incommensurate magnetic structure at T_{N2} and commensurate magnetic structure at T_{N1}.

Since the potential of practical applications of magnetoelectrics is usually considered in the context of magnetic memory and magnetic electronics, the low temperature of magnetic ordering seems to be the serious obstacle for implementation of the mulltiferroicity observed here. However, there is at least one niche for the low-temperature magnetoelectricity: the magnetic field sensors are competitive with SQUID even in the low temperature range [31]. Furthermore, the history of spin spiral multiferroics shows that the new mechanisms of magnetoelectric coupling, initially found in low-temperature materials, are also demonstrated at room temperatures.

Despite rapid progress in clarification of the basic mechanisms of magnetoelectric effects in solids, many aspects of these phenomena are to be clarified prior to the application stage. One of these aspects, i.e., coexistence and, possibly, mutual influence of mobile alkali ions with active magnetic and electric subsystems, is only touched on in the present study. Evidently, electric-polarization and neutron-scattering measurements of single crystals are necessary to establish the parameters of these structures at low temperatures. In addition, numerous representatives of the vast family of howardevansites are to be checked for possible multiferroicity.

ACKNOWLEDGMENTS

We acknowledge support of Russian Foundation for Basic research through joint Russia – India Project No. 17-52-45014. This work has been also supported by the Russian Ministry of Education and Science of the Russian Federation through NUST «MISiS» Grant No. К2-2017-084 and by the Act 211 of the Government of Russia, Contracts No. 02.A03.21.0004, No. 02.A03.21.0006, and No. 02.A03.21.0011.

[1] N. A. Hill, Why are there so few magnetic ferroelectrics?, J. Phys. Chem. B **104**, 6694 (2000).
[2] M. Fiebig, Revival of the magnetoelectric effect, J. Phys. D Appl. Phys. **38**, R123 (2005).
[3] W. Eerenstein, N. D. Mathur, and J. F. Scott, Multiferroic and magnetoelectric materials, Nature **442**, 759 (2006).
[4] M. Fiebig, T. Lottermoser, D. Meier, and M. Trassin, The evolution of multiferroics, Nat. Rev. Mater. **1**, 16046 (2016).
[5] K. F. Wang, J.-M. Liu, and Z. F. Ren, Multiferroicity: The coupling between magnetic and polarization orders, Adv. Phys. **58**, 321 (2009).
[6] S. Picozzi, K. Yamauchi, B. Sanyal, I. A. Sergienko, and E. Dagotto, Dual Nature of Improper Ferroelectricity in a Magnetoelectric Multiferroic, Phys. Rev. Lett. **99**, 227201 (2007).
[7] M. Lilienblum, T. Lottermoser, S. Manz, S. M. Selbach, A. Cano, and M. Fiebig, Ferroelectricity in the multiferroic hexagonal manganites, Nat. Phys. **11**, 1070 (2015).
[8] Y. Tokura, S. Seki, and N. Nagaosa, Multiferroics of spin origin, Rep. Prog. Phys. **77**, 76501 (2014).
[9] D. Khomskii, Multiferroics: Different ways to combine magnetism and ferroelectricity, J. Magn. Magn. Mater. **306**, 1 (2006).
[10] A. Ruff, A. Loidl, and S. Krohns, Multiferroic hysteresis loop, Materials **10**, 1318 (2017).
[11] S.-W. Cheong and M. Mostovoy, Multiferroics: A magnetic twist for ferroelectricity, Nat. Mater. **6**, 13 (2007).
[12] P. Barone and S. Picozzi, Mechanisms and origin of multiferroicity, Comptes Rendus Phys. **16**, 143 (2015).
[13] K. Dey, S. Majumdar, and S. Giri, Ferroelectricity in spiral short-ranged-ordered magnetic state of spinel $MnCr_2O_4$: Significance of topological frustration and magnetoelectric coupling, Phys. Rev. B **90**, 184424 (2014).
[14] T. Kimura, Y. Sekio, H. Nakamura, T. Siegrist, and A. P. Ramirez, Cupric oxide as an induced multiferroic with high-T-C, Nat. Mater. **7**, 291 (2008).
[15] J. M. Hughes, J. W. Drexler, C. F. Campana, and M. L. Malinconico, Howardevansite, $NaCu^{2+}Fe_2(^{3+})(VO_4)_3(^{3-})$, a new fumarolic sublimate from Izalco Volcano, El Salvador – Descriptive mineralogy and crystal-structure, Am. Mineral. **73**, 181 (1988).
[16] T. V. Drokina, G. A. Petrakovskii, O. A. Bayukov, A. M. Vorotynov, D. A. Velikanov, and M. S. Molokeev, Synthesis and structural, magnetic and resonance properties of the $LiCuFe_2(VO_4)_3$ compound, Phys. Solid State **58**, 1981 (2016).
[17] A. A. Belik, Synthesis and crystal structure of $LiCuFe_2(VO_4)_3$ by Rietveld method, Mater. Res. Bull. **34**, 1973 (1999).
[18] S. Kamusella and H.-H. Klauss, Moessfit a free Moessbauer fitting program, Hyperfine Interact. **237**, 82 (2016).
[19] G. A. Bain and J. F. Berry, Diamagnetic corrections and Pascal's constants, J. Chem. Educ. **85**, 532 (2008).
[20] M. G. Banks, R. K. Kremer, C. Hoch, A. Simon, B. Ouladdiaf, J. M. Broto, H. Rakoto, C. Lee, and M.-H. Whangbo, Magnetic ordering in the frustrated Heisenberg chain system cupric chloride $CuCl_2$, Phys. Rev. B **80**, 024404 (2009).
[21] W. Kleemann, Random fields in relaxor ferroelectrics – A jubilee review, J. Adv. Diel. **2**, 1241001 (2012).
[22] M. Salanne, D. Marrocchelli, and G. W. Watson, Cooperative mechanism for the diffusion of Li+ ions in $LiMgSO_4F$, J. Phys. Chem. C **116**, 18618 (2012).
[23] S. Kamoun, F. Hlel, and M. Gargouri, Electrical properties and conductivity mechanism of $LiCuFe_2(VO_4)_3$, Ionics **20**, 1103 (2014).

[24] W. Kohn and L. J. Sham, Self-consistent equations including exchange and correlation effects, Phys. Rev. A **140**, 1133 (1965).
[25] J. P. Perdew, K. Burke, and M. Ernzerhof, Generalized Gradient Approximation Made Simple, Phys. Rev. Lett. **77**, 3865 (1996).
[26] G. Kresse and J. Furthmuller, Efficient iterative schemes for ab initio total-energy calculations using a plane-wave basis set, Phys. Rev. B **54**, 11169 (1996).
[27] O. K. Andersen and T. Saha-Dasgupta, Muffin-tin orbitals of arbitrary order, Phys. Rev. B **62**, 16219 (2000).
[28] O. K. Andersen and O. Jepsen, Explicit 1-st Principles Tight-Binding Theory, Phys. Rev. Lett. **53**, 2571 (1984).
[29] V. I. Anisimov, I. V. Solovyev, M. A. Korotin, M. T. Czyzyk, and G. A. Sawatzky, Density-functional theory and NiO photoemission spectra, Phys. Rev. B **48**, 16929 (1993).
[30] C. N. R. Rao, A. Sundaresan, and R. Saha, Multiferroic and magnetoelectric oxides: The emerging scenario, J. Phys. Chem. Lett. **3**, 2237 (2012).
[31] Y. Wang, J. Li, and D. Viehland, Magnetoelectrics for magnetic sensor applications: Status, challenges and perspectives, Mater. Today **17**, 269 (2014).